1 January 2002

ELSEVIER

Optics Communications 201 (2002) 145–155

OPTICS COMMUNICATIONS

www.elsevier.com/locate/optcom

Compression of 2 mJ kilohertz laser pulses to 17.5 fs by pairing double-prism compressor: analysis and performance

Z. Cheng[a,*], F. Krausz[b], Ch. Spielmann[b]

[a] *Femtolasers Produktions GmbH, A-1040 Wien, Austria*
[b] *Institut für Photonik, Technische Universität Wien, A-1040 Wien, Austria*

Received 10 May 2001; received in revised form 24 August 2001; accepted 12 November 2001

Abstract

A general expression of dispersion for pairing double-prism compressor with arbitrary apex angle is presented and a limitation to generate negative group-delay dispersion (GDD) for broadband spectrum is obtained. By use of this compressor with spectral shaping filters and chirped mirrors, 2 mJ, 17.5 fs pulses from a compact 10-pass kilohertz Ti:sapphire amplifier system are generated.

1. Introduction

Chirped-pulse amplification (CPA) [1] has become a common technique for damage-free amplification of short pulses to terawatt levels and beyond. The development of ultrabroadband short pulse laser sources and application of CPA have resulted in a rapid progress in the development of high-intensity ultrashort pulse laser systems. The progress has opened the way to investigate and exploit a wide range of high-intensity and high-field phenomena in the intensity range 10^{15}–10^{19} W/cm^2 by use of small-scale laboratory systems. Successful amplification of ultrabroadband short pulse is mainly limited by two effects: uncompensated high-order dispersion in the amplifier system and gain narrowing in the amplifier media. The first effect can be minimized by a careful designed stretcher–compressor system [2,3]. Spectral shaping techniques permit the control of gain narrowing in ultrabroadband lasers. These techniques have been used to generate 10 TW 16 fs laser pulses at a 10 Hz repetition rate with two-stage Ti:sapphire amplifier [3] and 0.66 TW 21 fs laser pulses at a 1 kHz repetition rate with three-stage Ti:sapphire amplifier [4]. However, lossy grating-based pulse stretcher and pulse compressor not only add considerable complexity but require a higher overall gain to compensate for the losses and these setups make the entire system more complicated.

The pairing double-prism compressors have been used in intracavity [5] or extracavity [6,7] dispersion compensation for ultrashort pulse generation due to its advantages such as low loss, easy alignment and compactness. The negative group delay dispersions provided by a pair of prisms and

* Corresponding author. Tel.: +43-1-50370026; fax: +43-1-50370020.
E-mail address: zhao.cheng@femtolasers.com (Z. Cheng).

0030-4018/02/$ - see front matter
PII: S0030-4018(01)01675-3

double prisms are described by Duarte [8], Fork [9] and Sherriff [10], respectively. The results presented in the literatures [8–10] give only a GDD calculation for a reference wavelength (center wavelength) and the dispersion induced by the prism material is not included. However, with significant progress in the generation of ultrashort laser pulses, the dispersions over all ultrabroadband spectra are required. We present in Section 2 a general expression of group-delay dispersion (GDD) of a pair of double prisms for an arbitrary apex angle without the need for any approximation. This expression allows us to calculate the material dispersion resulting from insertion of the prism material into the beam and the angular dispersion. The high-order dispersion can also be calculated by means of this expression. Because the angular dispersion and the material dispersion in prism-pair have opposite signs, the limitation to generate negative GDD for ultrashort laser pulses due to broadband spectrum is also described in Section 2.

In order to investigate spectral gain narrowing and gain saturation, theoretical works have been published in more detail [11–14]. We follow a simplified model based on the transport equations [14] and numerically analyze our 10-pass chirped pulse amplifier with spectral gain narrowing and gain saturation. Additional experimental evidence is also provided for the analysis in Section 3.

In Section 4, we describe in more detail the performance of compressing 2 mJ kilohertz laser pulses to 17.5 fs by use of pairing double-prism compressor, compared to preliminary results [15]. A specially designed thin film structure having a wavelength-dependent attenuation (Gaussian spectral filter) is used for controlling spectral gain narrowing and a specially designed chirped mirrors provides compensation of high-order dispersion. Characterizations of compensated pulses by using techniques of fringe-resolved autocorrelation (FRAC) and second-harmonic generation frequency-resolved optical gating (SHG-FROG) are also reported. Another innovation in Section 4 is that a trigger signal for the pulse picker unit is supplied by the wings of seed spectrum leaking through a highly reflective mirror, instead of detecting photons from the overall seed spectrum in the previous system [7,15]. This improvement prevents narrowband or CW-induced optical damage to the amplifier crystal.

2. Pairing double-prism compressor

2.1. GDD for a pair of double prisms with an arbitrary apex angle

The GDD can be written as

$$\frac{\mathrm{d}^2\Phi(\omega)}{\mathrm{d}\omega^2} = \frac{\lambda^3}{2\pi c^2}\frac{\mathrm{d}^2P(\lambda)}{\mathrm{d}\lambda^2}, \tag{1}$$

where $P(\lambda)$ is the total optical path length, and $\Phi(\omega)$ is the overall spectral phase delay introduced by an optical system. In order to calculate the GDD of a pair of double prisms, we seek the expression of $P(\lambda)$.

A pair of double prisms is shown in Fig. 1(a). Four prisms with an identical apex angle α are arranged for minimum deviation of the reference wavelength λ_0 (the central wavelength). θ_i and ϕ_i (i from 1 to 8) denote the angles of incidence and refraction at eight interfaces. The phase delay from the plane P to the plane P' can be written in the form

$$P(\lambda) = AB + BC\cos\beta_1(\lambda) + CD\cos\beta_2(\lambda) + DE\cos\beta_3(\lambda) + EF. \tag{2}$$

Here we use the geometric optics theorem as employed by Fork [8]. And

$$\beta_1(\lambda) = \phi_2(\lambda) - \theta_1, \tag{3}$$

$$\beta_2(\lambda) = \delta_1 - \phi_4(\lambda), \tag{4}$$

$$\beta_3(\lambda) = \theta_7(\lambda) - \phi_8. \tag{5}$$

Inserting Eqs. (3)–(5) into Eq. (2) and making derivatives, we have

$$\frac{\mathrm{d}^2P(\lambda)}{\mathrm{d}\lambda^2} = l_1\left\{-\frac{\mathrm{d}^2\phi_2(\lambda)}{\mathrm{d}\lambda^2}\sin\beta_1(\lambda) - \left[\frac{\mathrm{d}\phi_2(\lambda)}{\mathrm{d}\lambda}\right]^2\cos\beta_1(\lambda)\right\}$$

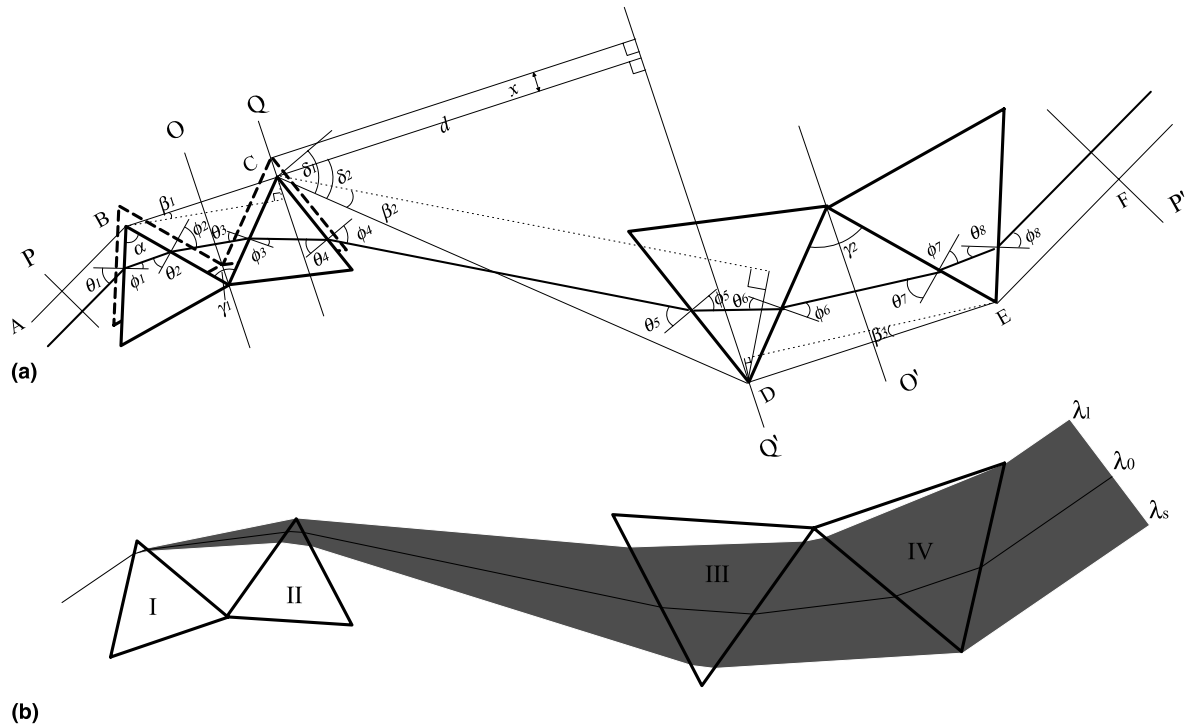

Fig. 1. Diagram of a pair of double prisms.

$$+ l_2\left\{ \frac{\mathrm{d}^2\phi_4(\lambda)}{\mathrm{d}\lambda^2}\sin\beta_2(\lambda) - \left[\frac{\mathrm{d}\phi_4(\lambda)}{\mathrm{d}\lambda}\right]^2\cos\beta_2(\lambda)\right\}$$

$$+ l_3\left\{ -\frac{\mathrm{d}^2\theta_7(\lambda)}{\mathrm{d}\lambda^2}\sin\beta_3(\lambda) - \left[\frac{\mathrm{d}\theta_7(\lambda)}{\mathrm{d}\lambda}\right]^2\cos\beta_3(\lambda)\right\}, \qquad (6)$$

where l_1, l_2, l_3 represent BC, CD and DE, respectively.

Assume that d is the perpendicular distance between two parallel planes Q and Q' which pass through the apexes C and D, respectively. Two planes Q and Q' are parallel to the symmetry axes O and O' of two prism pairs. In this case, when the prism pairs are translated along the axes O and O', d does not change.

For minimum deviation, $\theta_1 = \phi_8$, $\gamma_1 = \gamma_2 = 2\theta_1$ and $\sin\theta_1 = n(\lambda_0)\sin(\frac{1}{2}\alpha)$. And by inspection of Fig. 1(a), we can see that $\delta_1 = \delta_2 + (\alpha - \gamma_1/2) = \delta_2 + (\alpha - \theta_1)$, where $\cos\delta_2 = d/l_2$.

Using Snell's law and the relation $\alpha = \phi_1(\lambda) + \theta_2(\lambda) = \phi_3(\lambda) + \theta_4(\lambda) = \phi_5(\lambda) + \theta_6(\lambda) = \phi_7(\lambda) + \theta_8(\lambda)$ yields $\phi_2(\lambda) = \theta_7(\lambda)$ and $\beta_1(\lambda) = \beta_3(\lambda)$. Hence Eq. (6) can be rewritten by

$$\frac{\mathrm{d}^2P(\lambda)}{\mathrm{d}\lambda^2} = (l_1 + l_3)\left\{ \frac{\mathrm{d}^2\phi_2(\lambda)}{\mathrm{d}\lambda^2}\sin[\theta_1 - \phi_2(\lambda)] - \left[\frac{\mathrm{d}\phi_2(\lambda)}{\mathrm{d}\lambda}\right]^2\cos[\theta_1 - \phi_2(\lambda)]\right\}$$

$$+ l_2\left\{ \frac{\mathrm{d}^2\phi_4(\lambda)}{\mathrm{d}\lambda^2}\sin[\delta_1 - \phi_4(\lambda)] - \left[\frac{\mathrm{d}\phi_4(\lambda)}{\mathrm{d}\lambda}\right]^2\cos[\delta_1 - \phi_4(\lambda)]\right\}. \qquad (7)$$

And we obtain

$$\frac{\mathrm{d}\phi_2(\lambda)}{\mathrm{d}\lambda} = \frac{1}{\sqrt{1-n^2(\lambda)\sin^2\Theta 1(\lambda)}}\left\{\frac{\mathrm{d}n(\lambda)}{\mathrm{d}\lambda}\sin\Theta 1(\lambda) + \frac{\sin\theta_1}{n(\lambda)}\frac{\cos\Theta 1(\lambda)}{\sqrt{1-(\sin^2\theta_1/n^2(\lambda))}}\frac{\mathrm{d}n(\lambda)}{\mathrm{d}\lambda}\right\}, \tag{8}$$

$$\frac{\mathrm{d}\phi_4(\lambda)}{\mathrm{d}\lambda} = \frac{1}{\sqrt{1-n^2(\lambda)\sin^2\Theta 2(\lambda)}}\left\{\frac{\mathrm{d}n(\lambda)}{\mathrm{d}\lambda}\sin\Theta 2(\lambda) + \frac{\sin\Gamma(\lambda)}{n(\lambda)}\frac{\cos\Theta 2(\lambda)}{\sqrt{1-(\sin^2\Gamma(\lambda)/n^2(\lambda))}}\frac{\mathrm{d}n(\lambda)}{\mathrm{d}\lambda} + \cos\Gamma(\lambda)\frac{\cos\Theta 2(\lambda)}{\sqrt{1-(\sin^2\Gamma(\lambda)/n^2(\lambda))}}\frac{\phi_2(\lambda)}{\mathrm{d}\lambda}\right\}, \tag{9}$$

where

$$\Theta 1(\lambda) = \alpha - \arcsin\left(\frac{\sin\theta_1}{n(\lambda)}\right), \tag{10}$$

$$\Theta 2(\lambda) = \alpha - \arcsin\left(\frac{\sin\Gamma(\lambda)}{n(\lambda)}\right), \tag{11}$$

$$\Gamma(\lambda) = \gamma_1 - \phi_2(\lambda). \tag{12}$$

From Eqs. (8) and (9) one can obtain $\mathrm{d}^2\phi_2(\lambda)/\mathrm{d}\lambda^2$ and $\mathrm{d}^2\phi_4(\lambda)/\mathrm{d}\lambda^2$. Substituting Eqs. (8) and (9) into Eq. (7) yields an analytic expression. Therefore, using Eqs. (1) and (7) combined with Eqs. (8) and (9), one can calculate the exact wavelength-related dispersion, without the need for any approximation, for a pair of double prisms with an arbitrary apex angle. The high-order dispersion can be calculated by means of this expression. This expression also includes the change of dispersion resulting from a change in the insertion of the prism material into the beam by translating prism pairs along the axes O and O'. For instance, when the ray of reference wavelength λ_0 travels along A, B, C, D, E to F, the equations $\delta_1 = \theta_1$ and $\delta_2 = 2\theta_1 - \alpha$ are fulfilled (we call it a principal arrangement). In this case, there is no additional material dispersion included. When a prism pair is translated a distance of x to the direction of the apex, δ_2 changes from $2\theta_1 - \alpha$ to $\arctan\{[d\tan(2\theta_1 - \alpha) + x]/d\}$ and l_2 from

$$\sqrt{d^2 + d^2\tan^2(2\theta_1 - \alpha)}$$

to

$$\sqrt{d^2 + [d\tan(2\theta_1 - \alpha) + x]^2}.$$

In this case, the change of dispersion is not only from change of l_2 (to more negative), but also from change of δ_2 (to less negative). Actually, the change of dispersion resulting from the change of δ_2 is due to the change of the material dispersion.

It is interesting to note that (i) the dispersion induced by this system is contributed by three parts: two pairs of single prisms and one pair of double prisms (see Eq. (7)), (ii) in the principal arrangement mentioned above, the group-velocity dispersion (GVD) of a pair of double prisms (the second curled brackets in the right-hand side of Eq. (7)) is 2^2 times that of a pair of single prisms (the first curled brackets in the right-hand side of Eq. (7)) at the reference wavelength λ_0, but the third-order dispersion is not so, which means that this relation of the GVD is fulfilled only at the reference wavelength λ_0. As can be seen, $\theta_1 = \phi_2(\lambda_0)$, $\delta_1 = \phi_4(\lambda_0)$, in the principal arrangement, and

$$\left.\frac{\mathrm{d}\phi_4(\lambda)}{\mathrm{d}\lambda}\right|_{\lambda_0} = 2\left.\frac{\mathrm{d}\phi_2(\lambda)}{\mathrm{d}\lambda}\right|_{\lambda_0} = \frac{4}{n(\lambda_0)}\tan\theta_1\left.\frac{\mathrm{d}n(\lambda)}{\mathrm{d}\lambda}\right|_{\lambda_0}. \tag{13}$$

From Eqs. (1), (7) and (13), the above conclusion is obvious. Similarly, we can deduce that the GVD of a pair of triple prisms is 3^2 times that of a pair of single prisms at the reference wavelength λ_0 for the principal arrangement.

2.2. Limitation to generating negative GDD by a pair of double prism

As mentioned above, the dispersion introduced by this system contains no contribution of material in the principal arrangement. In this

case, the longer wavelength is dispersed outside the prism II by the prism I and the shorter wavelength is dispersed outside the prism III by the prisms I and II. So, the principal arrangement is unrealistic, especially for ultrabroadband pulses. In order to map an ultrabroadband spectra entirely inside the prisms, the two pairs of prisms are moved inversely along O and O'. The displacement of the first two prisms determines the longest wavelength inside prisms and that of the second two prisms determines the shortest wavelength inside the prisms, see Fig. 1(b). Owing to the insertion of prisms, the dispersion of material diminishes the generation of negative GDD by this system. For a certain separation of the prisms, the broader the spectrum, the lesser the magnitude of the negative GDD. Eventually a limited broadbandwidth spectrum is reached beyond which the total GDD dispersion at the center wavelength from Eq. (7) becomes positive no matter how large the distance d is. As a practical example, a calculation has been done by using the fused-silica prisms. In Fig. 2(a) GDD (at $\lambda_0 = 0.8$ μm) as a function of d for certain broadband spectra: $\lambda = 0.5$–1 μm, $\lambda = 0.542$–1 μm (the critical bandwidth) and $\lambda = 0.6$–1 μm, and (b) shows GDD (at $\lambda_0 = 0.8$ μm) versus the shortest wavelength λ_s for the distance $d = 0.5$ m, $d = 1$ m and $d = 1.5$ m. Fig. 3 shows GDD versus wavelength for different bandwidths $\lambda = 0.5$–1 μm, $\lambda = 0.542$–1 μm, $\lambda = 0.6$–1 μm and different distances $d = 0.5$ m, $d = 1$ m and $d = 1.5$ m, respectively.

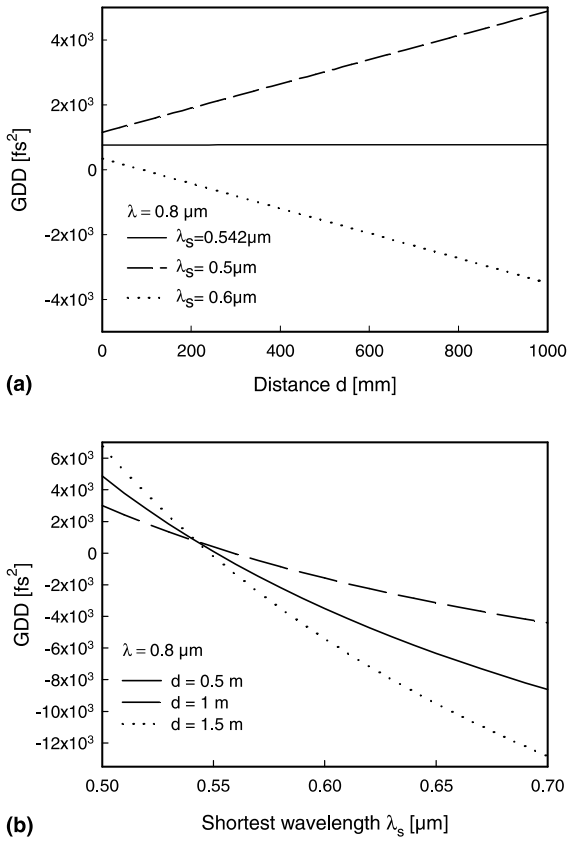

Fig. 2. (a) GDD (at $\lambda_0 = 0.8$ μm) as a function of d. (b) GDD (at $\lambda_0 = 0.8$ μm) versus the shortest wavelength λ_s.

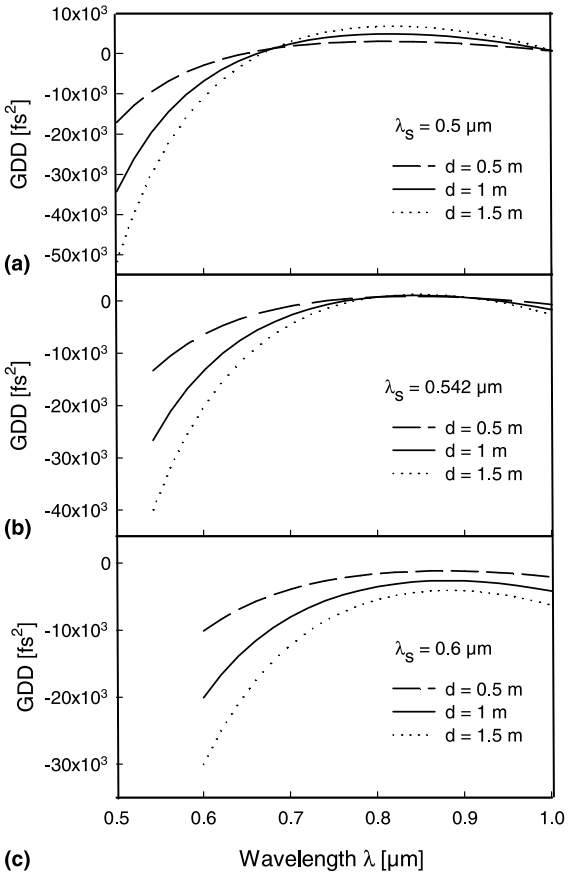

Fig. 3. GDD versus wavelength.

3. Numerical analysis of 10-pass amplifier

For simplicity, we consider gain saturation in time domain and spectral gain narrowing in frequency domain, respectively.

3.1. Gain saturation

Following a simplified model based on the transport equations [14]: the input intensity $I_{\text{in}}^{(n)}(t)$ and the output intensity $I_{\text{out}}^{(n)}(t)$ for the nth pass in the amplifier are related, for the multipass amplification, by

$$I_{\text{out}}^{(n)}(t) = G^{(n)}(t) I_{\text{in}}^{(n)}(t)(1-l). \tag{14}$$

Here l is the loss coefficient. And the nth pass instantaneous gain $G^{(n)}(t)$ is given in the form related to the time-dependent input energy fluence and the time-dependent output energy fluence as

$$G^{(n)}(t) = \frac{G_0^{(n)}}{G_0^{(n)} - (G_0^{(n)} - 1)\mathrm{e}^{-J_{\text{in}}^{(n)}(t)/J_{\text{sat}}}}, \tag{15}$$

where $G_0^{(n)} = G^{(n-1)}(\infty)$ denotes the final value of $G^{(n-1)}(t)$ after the pulse has passed. The time-dependent energy fluences (signal energies per unit area) are defined by

$$J_{\text{in}}^{(n)}(t) = \int_{-\infty}^{t} I_{\text{in}}^{(n)}(t)\,\mathrm{d}t, \tag{16}$$

$$J_{\text{out}}^{(n)}(t) = \int_{-\infty}^{t} I_{\text{out}}^{(n)}(t)\,\mathrm{d}t. \tag{17}$$

Here, $J_{\text{sat}} = \hbar\omega/\sigma$ is the saturation fluence. The input intensity for the nth pass is related to the output intensity for the $(n-1)$th pass by

$$I_{\text{in}}^{(n)}(t) = I_{\text{out}}^{(n-1)}(t). \tag{18}$$

Similarly, the input and output energy fluences for the nth pass have relations as

$$J_{\text{out}}^{(n)}(t) = J_{\text{sat}} \ln\left[\frac{G_0^{(n)} - 1}{G^{(n)}(t) - 1}\right], \tag{19}$$

$$J_{\text{in}}^{(n)}(t) = J_{\text{out}}^{(n-1)}(t). \tag{20}$$

In order to predict the gain saturation in our 10-pass system, we numerically solve Eqs. (14)–(20). Fig. 4 shows the instantaneous gain for the last five passes. For CPA, the instantaneous frequency related to the local time is also illustrated in Fig. 4.

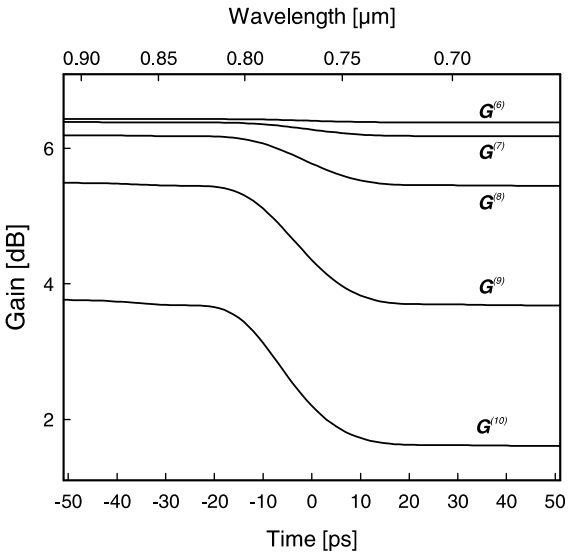

Fig. 4. Instantaneous gain for last five passes.

It can be seen from Fig. 4 that the leading edge of a pulse undergoes a higher gain than the trailing edge of the pulse. This effect distorts the input pulse to steepening of the leading edge and the pulse is distorted much more strongly with increasing the number of passes. Another effect which is caused by the gain saturation is the spectra red-shifting, particularly in the chirped-pulse amplification. In this case, the chirped pulse has a longer wavelength at the leading edge and a shorter wavelength at the trailing edge, so that the longer wavelength at the front of the pulse obtains a higher gain than the shorter wavelength at the tail of the pulse.

Fig. 5 shows the output energy versus the pass number n.

3.2. Gain narrowing

In the frequency domain, the atomic gain coefficient $\alpha_{\text{m}}(\omega)$ due to the atomic transition is given by [14]

$$\alpha_{\text{m}}(\omega) = \frac{1}{2}\sigma N \frac{1}{1 + [2(\omega - \omega_{\text{a}})/\Delta\omega_{\text{a}}]^2}, \tag{21}$$

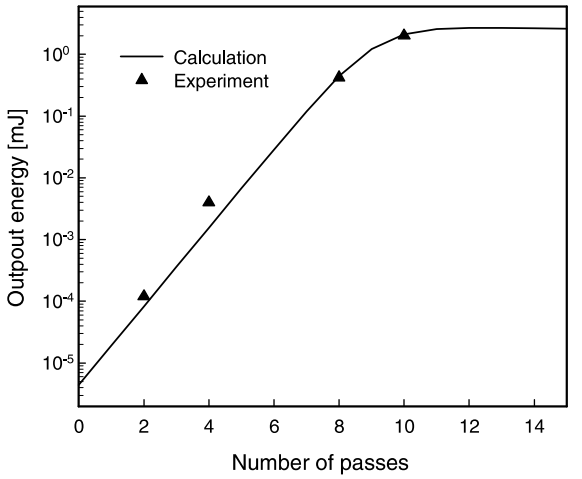

Fig. 5. Output energy as a function of pass number.

where ω_a is the atomic transition frequency, $\Delta\omega_a$ is the atomic linewidth, and N is the population inversion density.

The small signal power gain is

$$G(\omega) = \exp[2\alpha_m(\omega)l], \tag{22}$$

$$G(\omega) = \exp\left\{\sigma Nl \frac{1}{1 + [2(\omega - \omega_a)/\Delta\omega_a]^2}\right\}. \tag{23}$$

We neglect the gain saturation during single-pass amplification such that the small signal gain can be used for each of 10 passes. For the multipass amplification, the output spectrum $I_{out}^{(n)}(\omega)$, the input spectrum $I_{in}^{(n)}(\omega)$ and the gain $G^{(n)}(t)$ for the nth pass are related, analogizing to Eq. (14) by

$$I_{out}^{(n)}(\omega) = G^{(n)}(\omega) I_{in}^{(n)}(\omega). \tag{24}$$

The relationship between the amplified pulse spectrum $I_{out}(\omega)$ and the seed pulse spectrum $I_{in}(\omega)$ is given in the form

$$I_{out}(\omega) = I_{in}(\omega) \prod G^{(n)}(\omega). \tag{25}$$

The total gain $G_{tot}(\omega)$ is the product of all the single-pass small-signal gains $G^{(1)}(\omega)$ to $G^{(10)}(\omega)$ that is given by Eq. (23) with different N due to the gain saturation.

Because the frequency dependence of $\alpha_m(\omega)$ appears in the exponent of the gain expression 22, this leads to the gain bandwidth being narrower than the atomic linewidth and the narrowing increase with increasing the gain. This effect may decrease the gain bandwidth to 40 nm or less because of the huge value of the gain in multi-pass systems. In order to increase the amplified pulse spectrum, it is clear that a possibility is to shape the seed pulse spectrum with a frequency-dependent filter which has a larger attenuation at the peak of the gain than in the wings.

Considering the gain saturation as shown in Fig. 4, we calculate the amplified pulse spectra for two cases, with and without a spectral shaping filter. Fig. 6(a) shows the amplified and unamplified spectra without spectral shaping (dotted line). The amplified pulse spectrum and unamplified spectrum with spectral shaping (dotted line) are plotted in Fig. 6(b).

To provide additional evidence for the simplified model we present experimental data (full lines) in Figs. 5 and 6. The good agreement between the

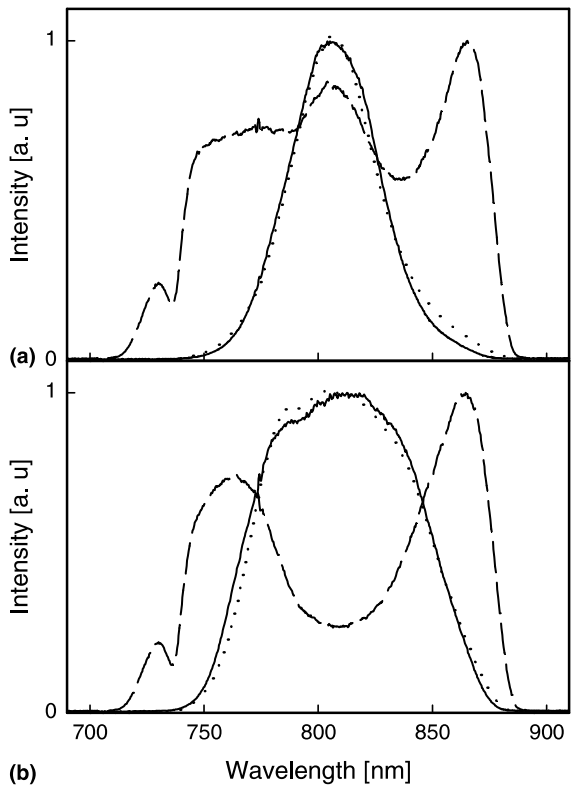

Fig. 6. Amplified and unamplified spectrum (a) without spectrum shaping and (b) with spectrum shaping.

calculated and experimental output energies in Fig. 5 as well as those of the measured and calculated spectra in Fig. 6 justifies this simplified model.

4. System performance

4.1. Layout

Our single-stage 10-pass oscillator–amplifier–compressor system shown in Fig. 7 is based on the previous system described in [7,15]. The front end of the system consists of a Kerr-lens mode-locked mirror-dispersion-controlled Ti:sapphire oscillator (FemtoSource Pro, FemtoLasers GmbH) delivering highly stable sub-10 fs pulses with a bandwidth of ≈ 150 nm. The typical spectrum (full line) and autocorrelation are shown in Fig. 8. The material dispersion of a 10 cm long slab of heavy flint glass (SF57, Schott) and other system components is sufficient to stretch the pulses up to ≈ 20 ps. The Gaussian spectral filter reshapes the pulse spectrum to diminish the gain narrowing effect. The chirped mirrors exhibiting positive third-order and fourth-order dispersions are exploited to eliminate high-order phase errors in the amplifier system. After the first-four-pass, the pre-amplified pulse train is extracted from the amplifier and passed through a pulse picker unit consisting of a Pockels-cell (PC) (Model 5046, Lasermetrics), a periscopic polarization rotator and a berek polarization compensator between two parallel polarizers. The pulse picker unit selects a single pulse at the peak of the envelope of the train of pre-amplified pulses by an adjustable delay and a timing between two trigger signals. One signal stems from a photodiode/Schmitt trigger unit which detects the pulse from the pump laser. To obtain the second signal representing the pulse train (MHz) of the oscillator, a fast photodiode detects the spectral components near the wings of the seed spectrum, which leaks through a steering mirror exhibiting a high reflectivity over the wavelength range 700–900 nm (dash line in Fig. 8(a)), instead of detecting photons from the overall spectral components of seed beam as used in the previous system [7,15]. Therefore, a narrowband seed pulses, which will not be broadened sufficiently by the stretcher, cannot trigger the pulse picker on. This innovation prevents the narrowband or CW-induced optical damage to the amplifier crystal.

The selected pulse is relaunched into the same arrangement in the reverse direction at a different altitude. After being amplified in another four passes, the pulse is passed through the periscopic telescope with a ratio of 2:1 and reinjected for the last two-pass amplifications which is arranged through the crystal between layers of the first-four-pass and those of the second-four-pass.

4.2. Performance

The amplifier is pumped by a cw-lamp-pumped, Q-switched, intracavity frequency-doubled Nd:YLF laser (Model 621D, BMI). To reduce the thermal lens, heat removal from the crystal is accomplished by a Peltier cooler attached to a water-cooled heat sink in a small vacuum chamber, by which the temperature in the crystal can be cooled down to $-30°$. At a pump pulse energy of 10 mJ, the output energies after 2, 4, 8 and 10 passes are in good agreement with our calculations, as shown in Fig. 5. The evolution of the train of pulses drained

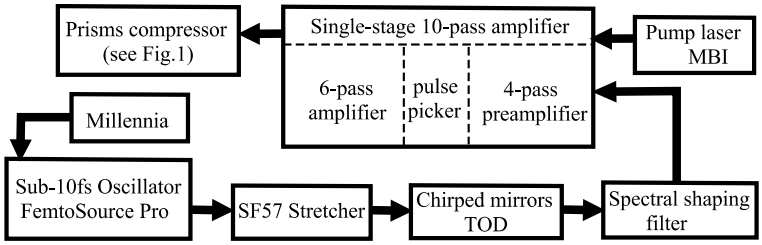

Fig. 7. Schematic of the laser system.

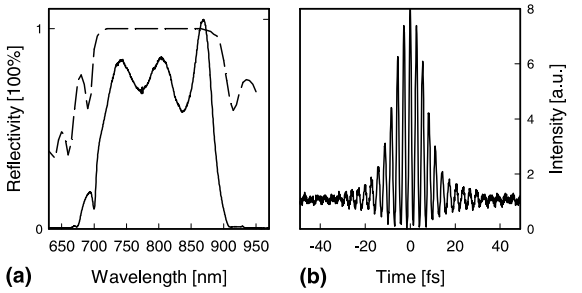

Fig. 8. (a) Seed pulse spectrum (full line). (b) Interferometric autocorrelation of seed pulse.

away from a polarizer in the pulse picker unit after being pre-amplified in the first four passes is shown in Fig. 9. Power amplification of the selected pulse (missing) picked out by the Pockels cell in additional (5–10) passes increasingly depletes the population inversion and reduces thereby the gain after the power amplification up to and including the 8th, 9th and 10th passes. (a), (b), (c) and (d) are the photographs of the train of pulses after the selected pulse is amplified in no more pass, four more passes, five more passes and six passes, respectively. The pulses are separated by the oscillator cavity round-trip time of 15 ns and the time delay between 4th pass and 10th pass is 25.1 ns. It means that the pulse only next to the selected one is amplified before the selected pulse is extracted in 10-pass amplifications. Fig. 9 clearly shows that only one pulse consumes the pump energy in the case of gain saturation.

The amplified pulse spectrum is plotted in Fig. 6(b) (full line). To demonstrate the effect of our Gaussian spectral filter, we remove the filter and measure the amplified pulse spectrum at the same output energy which is shown in Fig. 6(a) (full line). It clearly shows that the filter broadens the amplified pulse spectrum (FWHM) from 43 up to 78 nm.

The amplified pulses are passed through a pairing double fused silica prism compressor separated by 5.6 m. The throughput of the compressor is $\approx 90\%$. The group-delay dispersion of the compressor and the material dispersion introduced by the stretcher and other system components are shown in Fig. 10. The group-delay dispersion provided by chirped mirrors is also plotted in

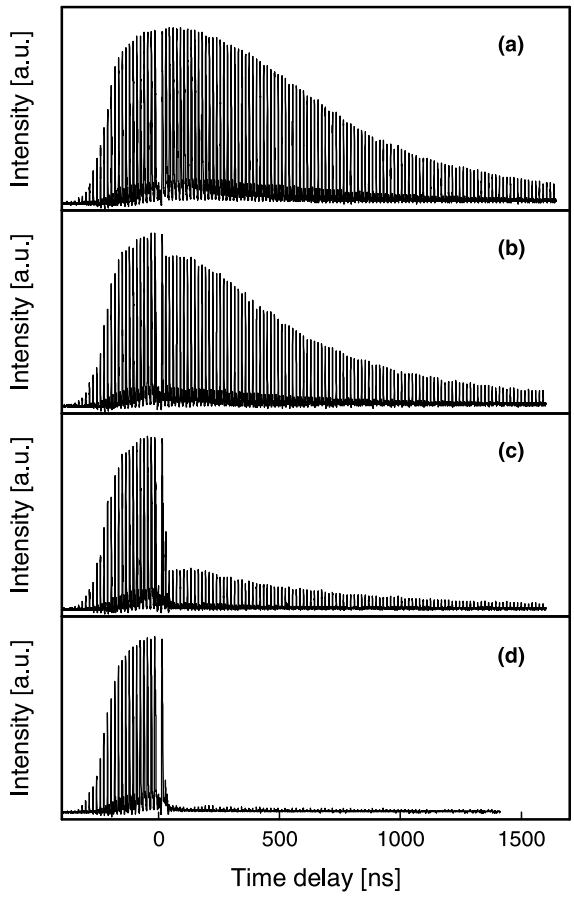

Fig. 9. The evolution of the train of pulses pre-amplified in first four passes through the amplifier: (a) the selected pulse (missing) has not been amplified in additional passes; (b) the selected pulse (missing) has been amplified in additional four passes (eight passes); (c) in additional five passes (nine passes) and (d) in additional six passes (10 passes).

Fig. 10. It clearly shows that the chirped mirrors with high-order dispersions can compensate the dispersion of the system up to the fourth order.

The recompressed pulses are characterized by the FRAC [16] and the SHG-FROG [17,18]. Our SHG-FROG correlator uses the same optical components and geometry (apart from a slight change from collinear to noncollinear recombination of the laser beams) as our fringe-resolved autocorrelator designed for high-fidelity measurement of sub-10 fs pulses. The beams (impinging at near normal incidence) are focused by a spherical mirror with a focal length of 7.5 cm onto the

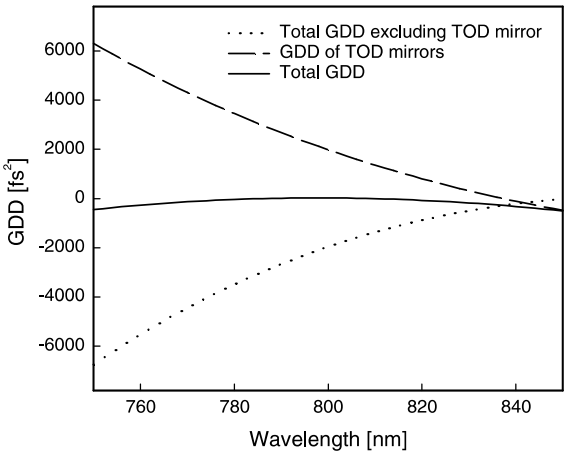

Fig. 10. Group-delay dispersion of the system.

20 μm KDP crystal. Due to the broad phase-matching bandwidth of KDP, our SHG-FROG apparatus allows the measurement of amplitude and chirp of high-energy near-infrared optical pulses with systematic errors being a factor of 3 smaller than an apparatus with BBO crystal. Fig. 12(a) shows the interferometric autocorrelation trace of the recompressed pulses having an energy of typically 2 mJ. Fig. 11 shows the contour plots of the measured and retrieved FROG traces of 17.5 fs pulse. The retrieved pulse shape and phase are shown in Fig. 12(b). The calculated Fourier transform limited pulse is also plotted in Fig. 12(b).

The beam diameter at the output of the prism compressor is ≈ 15 mm, keeping the nonlinear phase shifts in the prisms at a low level. In order to

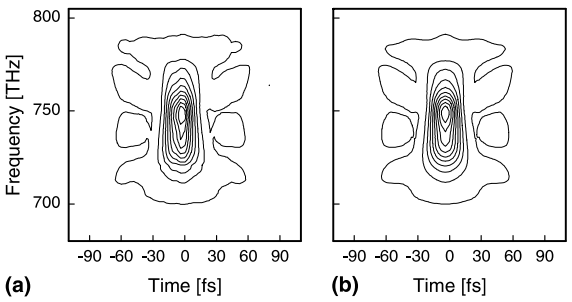

Fig. 11. (a) Measured and (b) retrieved FROG trace of a 17.5 fs pulse, The contour plots depict iso-intensity lines at the levels of $0.01 \times S_p$ and integer multiples of $0.1 \times S_p$, where S_p is the peak of $S(\omega, \tau)$.

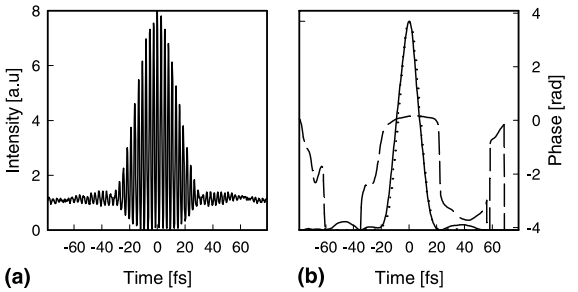

Fig. 12. (a) Interferometric autocorrelation of amplified pulse. (b) Retrieved pulse shape (full line), phase (dashed line) and transform-limited pulse shape (dotted line) from the measured spectrum.

assess the focusability of this beam, we characterized the beam. The beam is attenuated and gently focused by a lens of 1 m focal length. By measuring spot sizes versus propagation distance in the horizontal (x) and vertical (y) planes, respectively, we evaluate $M_x^2 = 1.5$ and $M_y^2 = 1.2$.

5. Summary

We have presented a general expression of dispersion of pairing double-prism compressor for arbitrary apex angle without the need of any approximation. This expression allows us to calculate the material dispersion resulting from an insertion of the prism material into the beam and the angular dispersion. A limitation to generate negative GDD for broadband spectrum has been obtained. By use of this compressor with spectral shaping filters and chirped mirrors, a compact single-stage 10-pass kilohertz Ti:sapphire amplifier which is able to generate 0.1 TW, 17.5 fs laser pulses has been demonstrated. The experimental results agree well with those expected by the use of a simplified model. The amplitude and chirp characterization of the pulses has been performed by FRAC and SHG-FROG measurement.

Recently developed commercially available compact system (Femtopower compact)[1] and

[1] www.femtolasers.com

demonstrated high-average-power system [19] produces 1 mJ 25 fs laser pulses requiring 1 m^2 space and 1.4 mJ 24 fs laser pulses requiring 1.5 m^2 space, respectively. We believe that using newly developed femtosource and chirped mirrors as well as new material prisms compressor will result in a reduction of the size of the overall system from 2 m^2 to 1 m^2 and permit the realization of unprecedentedly simplified and compact 0.1 TW kilohertz system.

Acknowledgements

This work was supported by the Jubilaeumsfonds der Oesterreichischen Nationalbank, grant # 6957.

References

[1] D. Strickland, G. Mourou, Opt. Commun. 56 (1985) 219.
[2] S. Backus, C. Durfee, G. Mourou, H.C. Kapteyn, M.M. Murnane, Opt. Lett. 22 (1997) 1256.
[3] K. Yamakawa, M. Aoyama, S. Matsuoka, H. Takuma, C.P.J. Barty, D. Fittinghoff, Opt. Lett. 23 (1998) 525.
[4] Y. Nabekawa, Y. Kuramoto, T. Togashi, T. Sekikawa, S. Watanabe, Opt. Lett. 23 (1999) 1384.
[5] U. Morgner, F.X. Kärter, S.H. Cho, Y. Chen, H.A. Haus, J.G. Fujimoto, E.P. Ippen, Opt. Lett. 24 (1999) 411–413.
[6] M. Nisoli, S. Stagiara, S. De Silvestri, O. Svelto, S. Sartania, Z. Cheng, M. Lenzner, Ch. Spielmann, F. Krausz, Appl. Phys. B 65 (1997) 189 (invited).
[7] S. Sartania, Z. Cheng, M. Lenzner, G. Tempea, Ch. Spielmann, F. Krausz, K. Ferencz, Opt. Lett. 22 (1997) 1562.
[8] F.J. Duarte, J.A. Piper, Opt. Commun. 43 (1982) 303.
[9] R.L. Fork, O.E. Martinez, J.P. Gordon, Opt. Lett. 9 (1984) 150.
[10] R.E. Sherriff, J. Opt. Soc. Am. B. 15 (1998) 1224.
[11] W.H. Lowdermilk, J.E. Murray, J. Appl. Phys. 51 (1980) 2435.
[12] Y.-H. Chuang, L. Zheng, D.D. Meyerhofer, IEEE J. Quant. Electron QE-29 (1993) 270.
[13] C. Le Blance, P. Curley, F. Salin, Opt. Commun. 131 (1996) 391.
[14] A.E. Siegman, Lasers, University Science Books, Mill Valley, CA, 1986.
[15] M. Hentschel, Z. Cheng, F. Krausz, Ch. Spielmann, Appl. Phys. B. 70 (2000) S161–S164.
[16] Ch. Spielmann, L. Xu, F. Krausz, Appl. Opt. 36 (1997) 2523.
[17] R. Trebino, D.J. Kane, JOSA A 10 (1993) 1101.
[18] Z. Cheng, A. Fürbach, S. Sartania, M. Lenzner, C. Spielmann, F. Krausz, Opt. Lett. 24 (2001) 247.
[19] S. Backus, R. Bartels, S. Thompson, R. Dollinger, H.C. Kapteyn, M.M. Murnane, Opt. Lett. 26 (2001) 465.